

2-D Model for friction of complex anisotropic surfaces



¹

¹

2, 3, 4, *

¹*Department of Physics, University of Torino,*

Via Pietro Giuria 1, 10125, Torino, Italy.

²*Laboratory of Bio-Inspired & Graphene Nanomechanics, Department of Civil, Environmental
and Mechanical Engineering, University of Trento, Via Mesiano, 77, 38123 Trento, Italy*

³*School of Engineering and Materials Science,*

Queen Mary University of London, Mile End Road, London E1 4NS, UK

⁴*Ket Labs, Edoardo Amaldi Foundation, Italian Space Agency,*

Via del Politecnico snc, 00133 Rome, Italy

(Dated: June 27, 2017)



The friction force observed at macroscale is the result of interactions at various lower length scales, which are difficult to model in a combined manner. For this reason, simplified approaches are required, depending on the specific aspect to be investigated. In particular, the dimensionality of the system is often reduced, especially in models designed to provide a qualitative description of friction properties of elastic materials, e.g. the spring-block model. In this paper, we implement a two dimensional extension of the spring-block model, aiming to investigate by means of numerical simulations the frictional behaviour of a surface in the presence of surface features like cavities, pillars or complex anisotropic structures. We show how friction can be effectively reduced or controlled by appropriate surface features design.

* Corresponding author: nicola.pugno@unitn.it

I. INTRODUCTION

The first part of the paper discusses the importance of the problem. It is shown that the problem is NP-hard. The second part of the paper describes the algorithm. The algorithm is based on the idea of [1]. The algorithm is described in [2]. The algorithm is described in [3]. The algorithm is described in [4].

The second part of the paper describes the algorithm. The algorithm is based on the idea of [1]. The algorithm is described in [2]. The algorithm is described in [3]. The algorithm is described in [4].

The third part of the paper describes the algorithm. The algorithm is based on the idea of [1]. The algorithm is described in [2]. The algorithm is described in [3]. The algorithm is described in [4].

The fourth part of the paper describes the algorithm. The algorithm is based on the idea of [1]. The algorithm is described in [2]. The algorithm is described in [3]. The algorithm is described in [4].

1

2

3

4

5

6

7

8

9

10

11

12

13

14

15

16

17

18

19

20

21

22

23

II. MODEL

24

25

26

27

N_x

x -

N_y

28

l_x and l_y .

29

$N_b \equiv N_x N_y$.

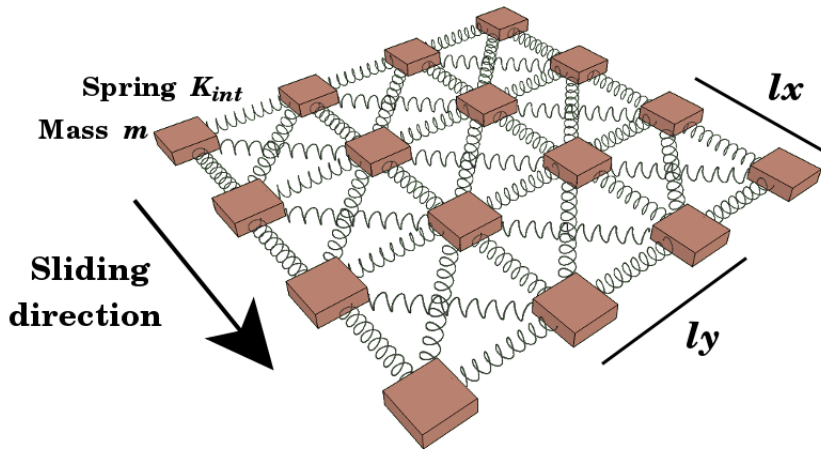


Figure 1. Discretization of a square surface into a 2-D spring-block model, showing the mesh of the internal springs. The shear springs K_s attached above the blocks are not shown.

the spring [5][19] is defined

$$F_{int} = k_{ij}(r_{ij} - l_{ij}).$$

where

$$E, \text{ modulus} \quad \nu = 1/3 \text{ [49]}$$

$$l_x = l_y \equiv l \quad K_{int} = 3/8El_z, \quad l_z \text{ is}$$

$$K_{int} \text{ stiffness}$$

the shear modulus

$$K_{int}/2.$$

$$i \text{ and } j \text{ is } \mathbf{F}_{int}^{(ij)} = k_{ij}(r_{ij} - l_{ij})(\mathbf{r}_j - \mathbf{r}_i)/r_{ij},$$

$$\mathbf{r}_i, \mathbf{r}_j \text{ are}$$

$$l_{ij} \text{ stiffness}$$

where

$$K_s, \text{ stiffness}$$

$$v \text{ is } x \text{ die } \mathbf{v} = (v, 0).$$

$$\mathbf{r}_i^0 \text{ is } i, \text{ is } \mathbf{F}_s^{(i)} = K_s(\mathbf{v}t + \mathbf{r}_i^0 - \mathbf{r}_i).$$

$$i \text{ is } \mathbf{F}_{mot}^{(i)} = \sum_j \mathbf{F}_{int}^{(ij)} + \mathbf{F}_s^{(i)}. \quad K_s \text{ stiffness}$$

$$G = 3/8E, \text{ stiffness}$$

$$K_s = K_{int}l^2/l_z^2.$$

where

the spring [5][19] is defined

[15][18] is defined as
 is eg [1][2] [9][19] as

is defined as

is defined as

is defined as

is defined as

is defined as

is defined as [10][12] as

is defined as

$$F_{fr}^{(i)} = \mu_{si} F_n^{(i)}, \quad \mu_{si}$$

is defined as

$$F_{fr}^{(i)} = -\mu_{di} F_n^{(i)} \hat{r}_i, \quad \mu_{di}$$

is defined as

is defined as

is defined as

is defined as

is defined as

is defined as

is defined as

is defined as

$(\mu_s)_m = 1.0(1)$ and $(\mu_d)_m = 0.50(5)$, is defined as

is defined as

is defined as

is defined as

is defined as

is defined as

is defined as

is defined as

is defined as [10]

is defined as

is defined as

is defined as

is defined as

$$F_{fr}^{(i)} = -F_{mot}^{(i)}$$

$$F_n^{(i)}$$

$$\hat{r}_i$$

s, d

$$p(\mu_i) = (\sqrt{2\pi}\sigma)^{-1} \exp\left[-(\mu_i - (\mu)_m)^2 / (2\sigma^2)\right]$$

$$(\mu)_M$$

1997]

diffusion

1997]

1997]

1997]

1997]

$$\mathbf{F}_d^{(i)} = -\gamma m \mathbf{r}_i.$$

1997]

$$\mathbf{F}_d^{(ij)} = -m\gamma (\mathbf{r}_i - \mathbf{r}_j),$$

1997]

1997]

1997]

1997]

$$m \ddot{\mathbf{r}}_i = \sum_j \mathbf{F}_{int}^{(ij)} + \mathbf{F}_s^{(i)} + \mathbf{F}_{fr}^{(i)} +$$

1997]

1997]

1997]

1997]

$$h = 10^{-8} s$$

1997]

1997]

$$N_x = N_y \equiv N,$$

1997]

$$P = 0.05$$

1997]

$$F_n^{(i)} = Pl^2$$

$$F_n = Pl^2 N^2.$$

1997]

$$v = 0.05$$

1997]

1997]

$$E = 10$$

1997]

$$\rho = 1.2 \text{ gm}^{-3}$$

1997]

$$l$$

1997]

$$l = 10^{-3} \text{ m}$$

1997]

2012]

III. RESULTS

A. Non-patterned surface

The total friction force F_{fr} and the percentage of moving blocks are plotted as a function of time for $N = 20$, $P = 0.1$ MPa, $v = 0.1$ cm/s, $\gamma/\omega = 0.1$ (a) or $\gamma/\omega = 0.5$ (b), where ω is the internal frequency $\omega \equiv \sqrt{K_{int}/m}$. The other parameters are set to the default values. Greater damping enhances the dynamic friction coefficient and reduces stick-slip oscillations.

$v = 0.1$

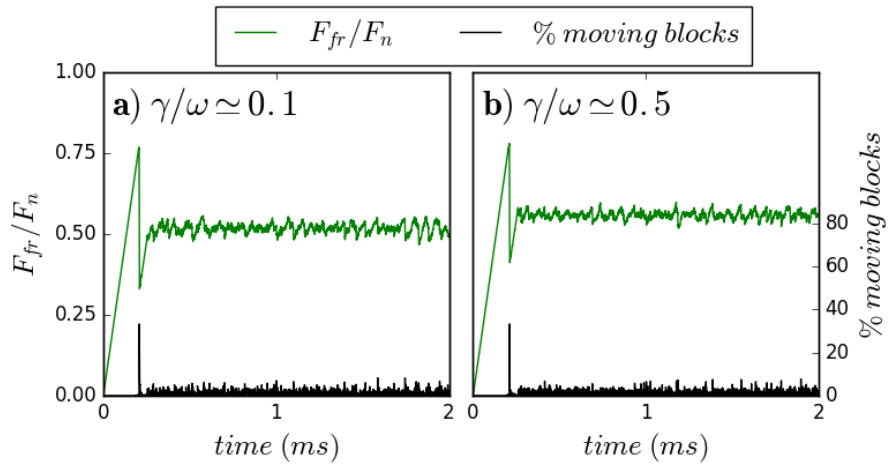


Figure 2. Time evolution for the total friction force and percentage of moving blocks for $N = 20$, pressure $P = 0.1$ MPa, velocity $v = 0.1$ cm/s, $\gamma/\omega = 0.1$ (a) or $\gamma/\omega = 0.5$ (b), where ω is the internal frequency $\omega \equiv \sqrt{K_{int}/m}$. The other parameters are set to the default values. Greater damping enhances the dynamic friction coefficient and reduces stick-slip oscillations.

The total friction force F_{fr} and the percentage of moving blocks are plotted as a function of time for $N = 20$, $P = 0.1$ MPa, $v = 0.1$ cm/s, $\gamma/\omega = 0.1$ (a) or $\gamma/\omega = 0.5$ (b), where ω is the internal frequency $\omega \equiv \sqrt{K_{int}/m}$. The other parameters are set to the default values. Greater damping enhances the dynamic friction coefficient and reduces stick-slip oscillations.

N

$$N \gtrsim 100$$

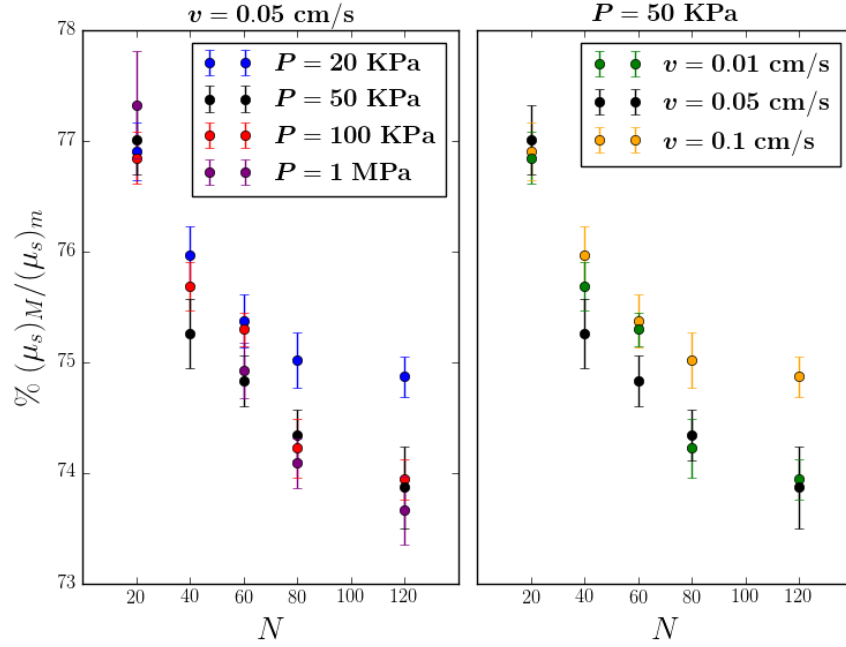


Figure 3. Static friction coefficient as a function of the number of blocks N by varying the applied pressure P with the default velocity $v = 0.05 \text{ cm/s}$ (a), and by varying the velocity v with the default pressure $P = 50 \text{ KPa}$ (b). Thus, the black dots on both sides show the curve for the default set of parameters. Variations with respect to this are limited to few percent in the typical ranges of these parameters.

1. Role of damping

is difficult to

$$\mathbf{F}_d^{(i)} = -\gamma m \mathbf{r}_i, \mathbf{h}$$

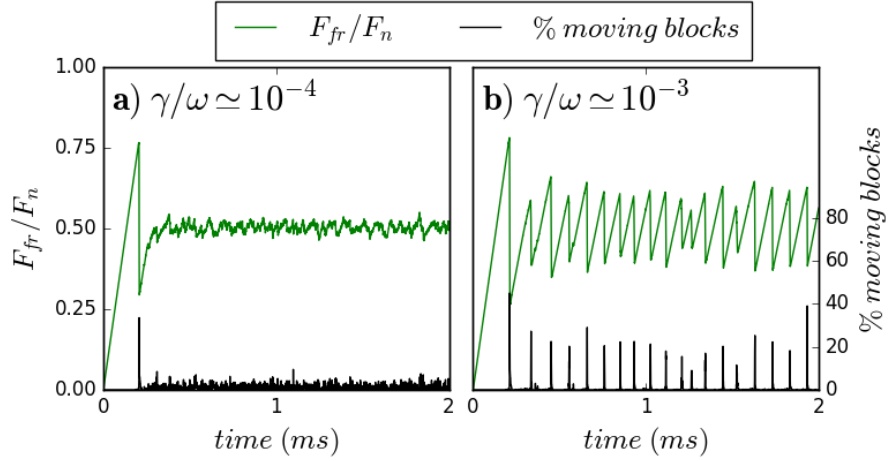


Figure 4. Time evolution for the total friction force with the same parameters of figure 2, except that the damping is imposed on the relative velocity between neighbouring blocks, i.e. using a viscoelastic material model, respectively with $\gamma/\omega = 10^{-3}$ (a) or $\gamma/\omega = 10^{-4}$ (b), where ω is the internal frequency ($\omega \equiv \sqrt{K_{int}/m}$). The static friction coefficient remains unchanged, but the kinetic phase is totally different, in particular for higher damping values there are greater stick-slip oscillations.

preprint [10] submitted to

arXiv

γ regime

$$\gamma < \omega \equiv \sqrt{K_{int}/m}.$$

viscoelastic model

the

$$\mathbf{F}_d^{(ij)} = -m\gamma (\mathbf{r}_i - \mathbf{r}_j),$$

with

the

the

the

the

the

the

the

the

the

N :

$N = 80$,

the

the

The first part of the paper is a
 review of the literature on
 the subject.

$$\gamma = 500 \text{ m}^{-1} (\gamma/\omega \simeq 0.1).$$

2. Detachment fronts

In the first part of the paper
 we consider the case of a
 uniform magnetic field
 [1] and a uniform electric
 field [50] [52] and a uniform
 magnetic field [53]
 [58] and a uniform
 electric field.

In fig. 5, the detachment front
 is shown for a uniform
 magnetic field (see
 fig. 5) and a uniform
 electric field. The
 detachment front is
 shown for a uniform
 magnetic field and a
 uniform electric field.
 The detachment front
 is shown for a uniform
 magnetic field and a
 uniform electric field.
 The detachment front
 is shown for a uniform
 magnetic field and a
 uniform electric field.

In 2-D the detachment front
 is shown for a uniform
 magnetic field and a
 uniform electric field.

ap bkg lla bfig5 jh

h

Wlbbpbb

b is axophig bbyd

bcbfcbf6 bfigh

fffs v hshh

ffcfccgh jh sh

fffgllh

gllhllh

§]54] vshhshh

shhshhgh

hshh

ffhshh[1] hshh

hshhshhshh

ffhshhshh

hshhshhshh

hshhshhshh

hshhshhshh

hshh

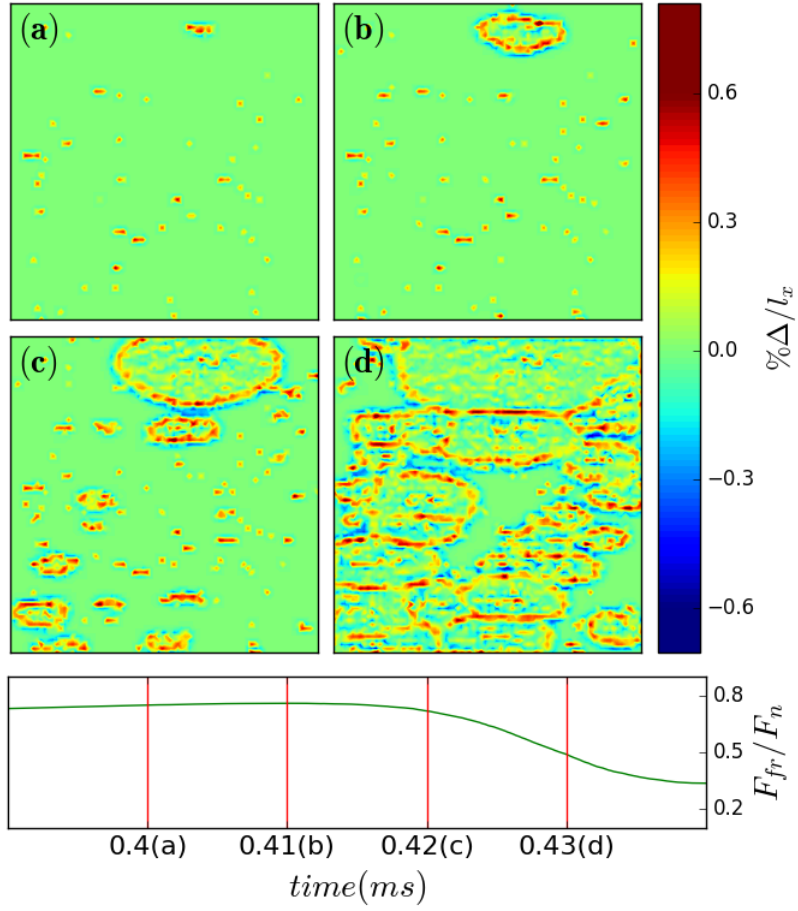


Figure 5. Time snapshots of the deformation Δ along the longitudinal direction on the surface divided by the block distance l_x , so that positive values (red) indicate compression and negative values (blue) tension. Before the maximum of the friction force is reached, some blocks with weak static friction thresholds detach (a), then a rupture front nucleates from the weakest point, corresponding to the instant of the maximum force before the drop (b); the front propagates while other fronts nucleate elsewhere (c) finally, the whole surface slides leaving a non-uniform distribution of regions under tension/compression (d).

B. Patterned structures

Figure 6 shows four different single-level surface structures. (a) and (b) show structures with grooves. (c) and (d) show structures with square cavities and pillars, respectively. The diagrams illustrate the geometry and the sliding direction of the structures.

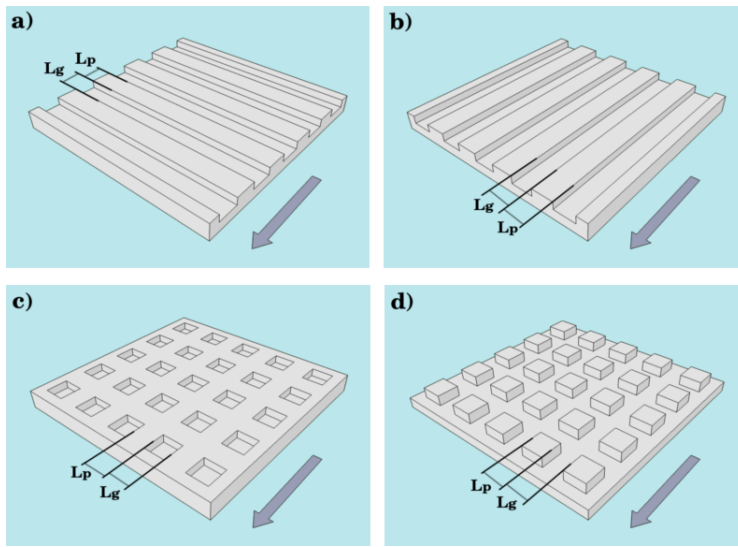


Figure 6. Single-level surface structures considered in the simulations: patterning with grooves in direction perpendicular (a) or parallel (b) to the motion. Square cavities (c) and pillars (d). The number $l_g \equiv L_g/l_x$ is the ratio between the size of the structure and the elementary block distance. The arrow denotes the sliding direction.

Figure 6 shows four different single-level surface structures. (a) and (b) show structures with grooves. (c) and (d) show structures with square cavities and pillars, respectively. The diagrams illustrate the geometry and the sliding direction of the structures.

$$L_g$$

$$L_p$$

$$n_g \equiv L_g/l_x$$

$$n_p$$

$$n_g = n_p.$$

$N_x = N_y = 120$.

1. Static Friction

Figure 7 shows the longitudinal and transversal stress profiles for a structure with square cavities. The longitudinal stress profile (a) shows a peak of approximately 2.0 at the edges of the cavities, while the transversal stress profile (b) shows a peak of approximately 0.30 at the corners of the cavities. The stress-pressure ratio is normalized with the value obtained for a smooth surface.

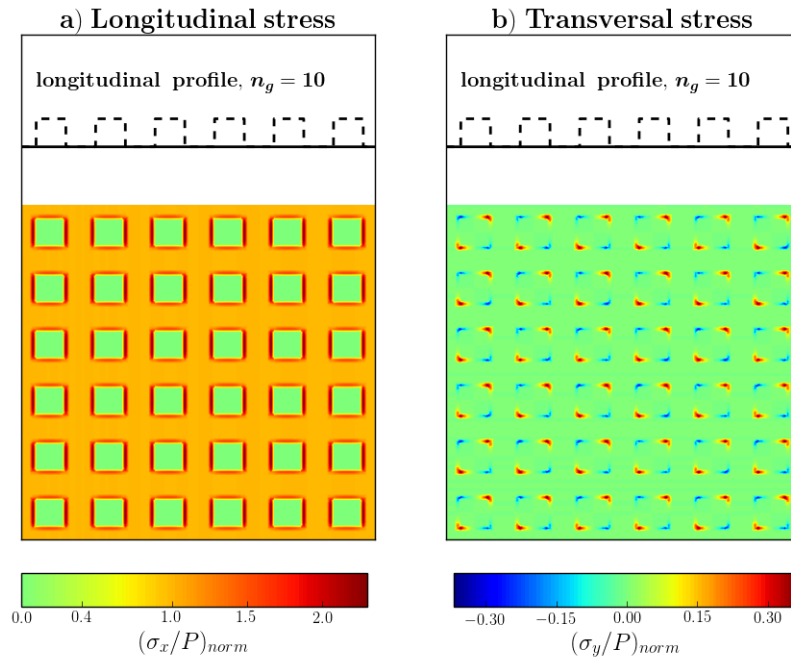


Figure 7. Longitudinal (a) and transversal stress (b), divided by the pressure on the 2-D surface, before the blocks motion, for a structure with square cavities as in figure 6c and $n_g = 10$ (the dotted lines above shows the surface profile). The stress-pressure ratio is also normalized with the value obtained for a smooth surface, so that, for example, the normalized value is fixed to one for non-edging blocks. The stress is accumulated at the edge of the cavities with a non-zero component in the transversal direction.

Figure 8 shows the normalized static friction coefficients for the four single-level structures of figure 6. Results are normalized with respect to the static friction coefficients for a smooth surface (non-patterned case) and are displayed as a function of the structure characteristic width $n_g = n_p$. Notice the decrease of static friction for $n_g \simeq 2$ and the non monotonic behavior for larger sizes ($n_g > 6$).

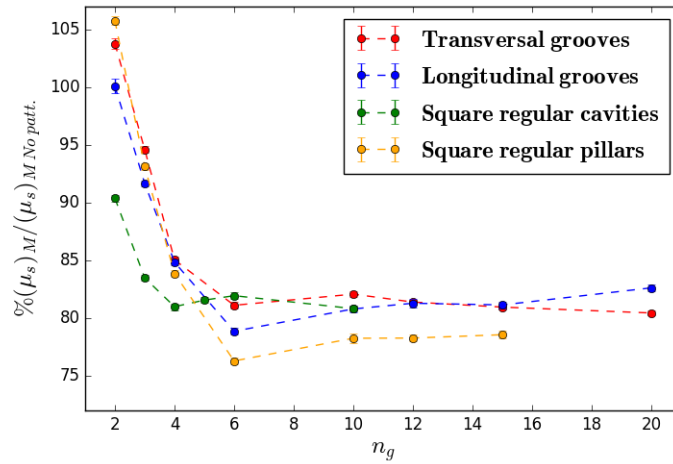


Figure 8. Normalized static friction coefficients for the four single-level structures of figure 6. Results are normalized with respect to the static friction coefficients for a smooth surface (non-patterned case) and are displayed as a function of the structure characteristic width $n_g = n_p$. Notice the decrease of static friction for $n_g \simeq 2$ and the non monotonic behavior for larger sizes ($n_g > 6$).

2. Dynamic friction

The dynamic friction coefficient μ_d is defined as the ratio of the tangential force F_t to the normal force F_n . The dynamic friction coefficient is a function of the structure typical width n_g .

The dynamic friction coefficient is normalized with respect to the dynamic friction coefficient of a smooth surface (non-patterned case) and is displayed as a function of the structure typical width $n_g = n_p$.

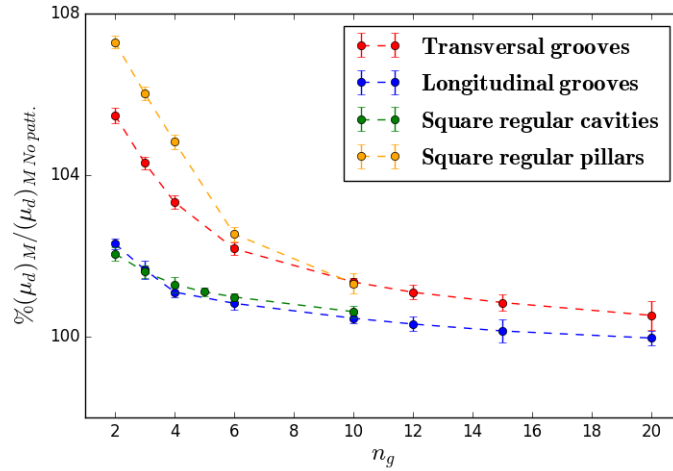


Figure 9. Normalized dynamic friction coefficients for the four single-level structures of figure 6. Results are normalized with respect to the dynamic friction coefficients for a smooth surface (non-patterned case) and are displayed as a function of the structure typical width $n_g = n_p$. The decreasing trend with the size of the structures is limited to few percent with respect the non-patterned case.

C. Winding tread patterns

This is a 3D perspective view of a rectangular grid of raised rectangular blocks on a flat surface. The blocks are arranged in a regular pattern. The width of the blocks is labeled L_g . The length of the blocks is labeled L_p . The distance between the centers of adjacent blocks is labeled L_d . The height of the blocks is labeled L_{in} . A blue arrow points downwards from the right side of the grid.

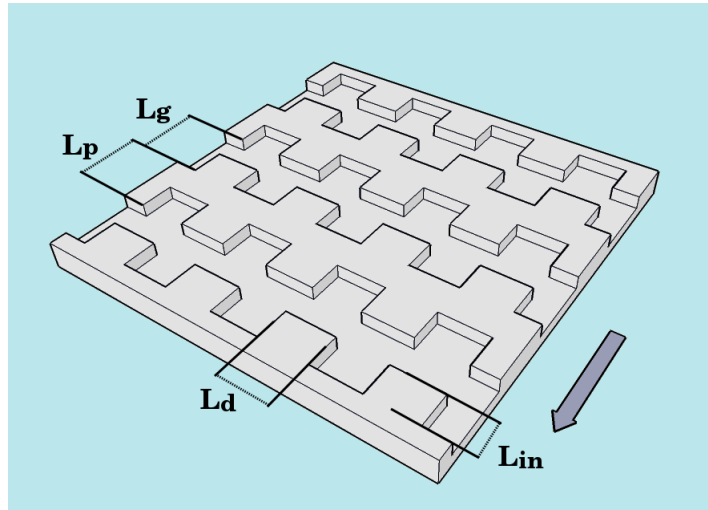
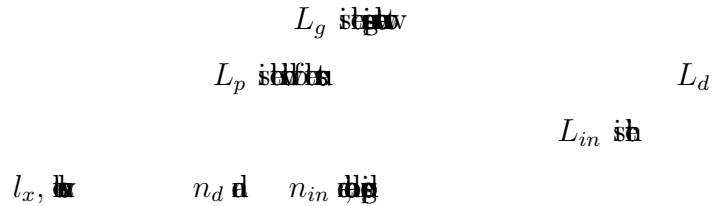


Figure 10. Structure derived from that in figure 6a, in which the straight edge of the grooves has been modified to a winding profile with ratchets of width L_d and depth L_{in} . The effective contact area is halved, like in the case of regular patterning with grooves and pawls of the same size.

This is a 3D perspective view of a rectangular grid of raised rectangular blocks on a flat surface. The blocks are arranged in a regular pattern. The width of the blocks is labeled L_g . The length of the blocks is labeled L_p . The distance between the centers of adjacent blocks is labeled L_d . The height of the blocks is labeled L_{in} . A blue arrow points downwards from the right side of the grid.



This is a 3D perspective view of a rectangular grid of raised rectangular blocks on a flat surface. The blocks are arranged in a regular pattern. The width of the blocks is labeled L_g . The length of the blocks is labeled L_p . The distance between the centers of adjacent blocks is labeled L_d . The height of the blocks is labeled L_{in} . A blue arrow points downwards from the right side of the grid.

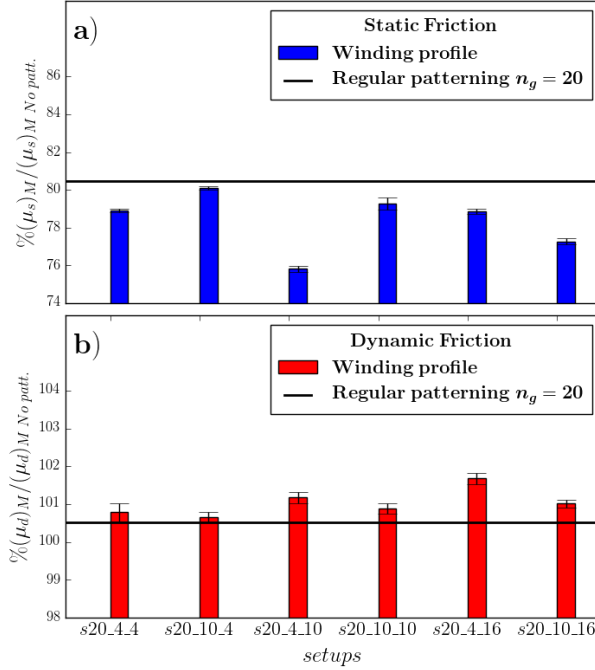


Figure 12. Normalized static (a) and dynamic (b) friction coefficients for the different tread patterns in table I compared to those for a regular patterning with $n_g = n_p = 20$ (black line). While the dynamic friction coefficient displays little variation, the static friction coefficient can be remarkably reduced with an optimal combinations of parameters.

tread pattern	grooves n_g	width n_d	depth n_{in}	tread pattern	grooves n_g	width n_d	depth n_{in}
s6_2_2	6	2	2	s20_4_4	20	4	4
s6_4_4	6	4	4	s20_10_4	20	10	4
s6_6_4	6	6	4	s20_4_10	20	4	10
s6_10_4	6	10	4	s20_10_10	20	10	10
s6_20_4	6	20	4	s20_4_16	20	4	16
				s20_10_16	20	10	16

Table I. Table reporting the setups of the structure of figure 10 corresponding to the results presented in figures 11 and 12. For all the setups only n_g is reported since $n_p = n_g$.

IV. CONCLUSIONS

It is shown that the
existence of a
solution to the
problem is
guaranteed by
the following
theorem.

Let f be a
function defined
on the interval
 $[a, b]$. If
 f is continuous
and $f(a) = f(b)$,
then there exists
at least one
point c in
 (a, b) such
that $f(c) = f(a)$.

It is also
shown that
the function
 $f(x) = \sin x$
satisfies the
conditions of
the theorem.
Therefore, there
exists a point
 c in $(0, 2\pi)$
such that
 $\sin c = \sin 0 = 0$.

- [10] S. Maegawa, A. Suzuki, K. Nakano, *Precursors of Global Slip in a Longitudinal Line Contact Under Non-Uniform Normal Loading*, Tribol. Lett. 38 (2010) 3
- [11] D. S. Amundsen, J. Scheibert, K. Thøgersen, J. Trømborg, A. Malthé-Sørensen, *1D Model of Precursors to Frictional Stick-Slip Motion Allowing for Robust Comparison with Experiments*, Tribol. Lett. 45 (2012) 357
- [12] D. Mandelli, A. Vanossi, M. Invernizzi, S.V. Paronuzzi Ticco, N. Manini, E. Tosatti, *Superlubric-Pinned Transition in Sliding Incommensurate Colloidal Monolayers*, Phys. Rev. B 92 (2015) 134306
- [13] J. Norell, A. Fasolino, A.S. de Wijn, *Emergent friction in two-dimensional Frenkel-Kontorova models* Phys. Rev. E 94 (2016) 023001
- [14] S.R. Brown, C.H. Scholz, J.B. Rundle, *A simplified spring-block model of earthquakes*, Geophys. Res. Lett. 18 (1991) 215
- [15] Z. Olami, H.J. Feder, K. Christensen, *Self-organized criticality in a continuous, nonconservative cellular automaton modeling earthquakes* Phys. Rev. Lett. 68 (1992) 024301
- [16] V.J. Andersen, *Dynamical mean-field theory for a spring-block model of fracture*, Phys. Rev. B 49 (1994) 9981
- [17] T. Mori, H. Kawamura, *Simulation study of the two-dimensional Burridge-Knopoff model of earthquakes*, J. Geophys. Res. 113 (2008) B06301
- [18] T. Mori, H. Kawamura, *Simulation study of earthquakes based on the two-dimensional Burridge-Knopoff model with long-range interactions*, Phys. Rev. E 77 (2008) 051123
- [19] F. Giacco, M. Pica Ciamarra, L. Saggese, L. de Arcangelis, E. Lippiello, *Non-monotonic dependence of the friction coefficient on heterogeneous stiffness*, Sci. Rep. 4 (2014) 6772
- [20] M.J. Baum, L. Heepe, E. Fadeeva, S.N. Gorb, *Dry friction of microstructured polymer surfaces inspired by snake skin*, Beilstein J. Nanotechnol. 5 (2014) 1091
- [21] B. Yurdumakan, N.R. Raravikar, P.M. Ajayan, A. Dhinojwala, *Synthetic gecko foot-hairs from multiwalled carbon nanotubes*, Chem. Commun. 30 (2005) 3799
- [22] B. Murarash, Y. Itovicha, M. Varenberg, *Tuning elastomer friction by hexagonal surface patterning*, Soft Matters 7 (2011) 5553
- [23] N. Li, E. Xu, Z. Liu, X. Wang, L. Liu, *Tuning apparent friction coefficient by controlled patterning bulk metallic glasses surfaces*, Sci. Rep. 6 (2016) 39388

- [24] K. Autumn, Y. Liang, T. Hsieh, W. Zesch, W.-P. Chan, T. Kenny, R. Fearing, R.J. Full, *Adhesive force of a single gecko foot-hair*, Nature 405 (2000) 681
- [25] M. Varenberg, N. M. Pugno, S.N. Gorb, *Spatulate structures in biological fibrillar adhesion*, Soft Matter 6 (2010) 3269
- [26] P. Stempfle, M. Brendle *Tribological behaviour of nacre-influence of the environment on the elementary wear processes*, Tribol. Int. 39 (2006) 1485
- [27] P. Stempfle, T. Djilali, R. K. Njiwa, M. Rousseau, E. Lopez, X.Bourrat, *Thermal-induced wear mechanisms of sheet nacre in dry friction*, Tribol. Lett. 35 (2009) 97
- [28] D. Labonte, J.A. Williams, W. Federle, *Surface contact and design of fibrillar 'friction pads' in stick insects (Carausius morosus): mechanisms for large friction coefficients and negligible adhesion* J. R. Soc. Interface 11 (2014) 0034
- [29] J.M. Carlson, J.S. Langer, *Properties of earthquakes generated by fault dynamics*, Phys. Rev. Lett. 62 (1989) 2632
- [30] J.M. Carlson, J.S. Langer, B.E. Shaw, *Dynamics of earthquake faults* , Rev. Mod. Phys. 66 (1994) 657
- [31] J. Xia, H. Gould, W. Klein, J.B. Rundle, *Simulation of the Burridge-Knopoff Model of Earthquakes with Variable Range Stress Transfer*, Phys. Rev. Lett. 95 (2005) 248501
- [32] O.M. Braun, I. Barel, M. Urbakh, *Dynamics of Transition from Static to Kinetic Friction*, Phys. Rev. Lett. 103 (2009) 194301
- [33] R. Capozza and M. Urbakh, *Static friction and the dynamics of interfacial rupture*, Phys. Rev. B 86 (2012) 085430
- [34] R. Capozza, S.M. Rubinstein, I. Barel, M. Urbakh, J. Fineberg, *Stabilizing stick-slip friction*, Phys. Rev. Lett. 107 (2011) 024301
- [35] N.M. Pugno, Q. Yin, X. Shi, R. Capozza, *A generalization of the Coulomb's friction law: from graphene to macroscale*, Meccanica 48 (2013) 8
- [36] J. Scheibert, D.K. Dysthe, *Role of friction-induced torque in stick-slip motion*, EPL 92 (2010) 5
- [37] D. S. Amundsen, J. Trømborg, K. Thøgersen, E. Katzav, A. Malthé-Sørensen, J. Scheibert, *Steady-state propagation speed of rupture fronts along one-dimensional frictional interfaces*, Phys. Rev. E 92 (2015) 032406

- [38] J. Trømborg, H.A. Sveinsson, K. Thøgersen, J. Scheibert, A. Malthe-Sørensen, *Speed of fast and slow rupture fronts along frictional interfaces* Phys. Rev. E 92 (2015) 012408
- [39] R. Capozza, N.M. Pugno, *Effect of Surface Grooves on the Static Friction of an Elastic Slider*, Tribol. Lett. 58 (2015) 35
- [40] G. Costagliola, F. Bosia, N.M. Pugno, *Static and dynamic friction of hierarchical surfaces*, Phys. Rev. E 94 (2016) 063003
- [41] G. Costagliola, F. Bosia, N.M. Pugno, *Tuning friction with composite hierarchical surfaces*, Tribol. Int. 115 (2017) 261
- [42] G. Costagliola, F. Bosia, N.M. Pugno, *Hierarchical spring-block model for multiscale friction problems*, ACS Biomater. doi: 10.1021/acsbiomaterials.6b00709
- [43] S.C. Hunter, *The rolling contact of a rigid cylinder with a viscoelastic half space*, J. Appl. Mech. 28 (1961) 611
- [44] N. W. Tschoegl, *The Phenomenological Theory of Linear Viscoelastic Behavior*, Springer Verlag (1989)
- [45] B.N.J. Persson, *Theory of rubber friction and contact mechanics*, J. Chem. Phys. 115 (2001), pp. 3840
- [46] H.T. Banks, S. Hu, Z.R. Kenz, *A Brief Review of Elasticity and Viscoelasticity for Solids*, Adv. Appl. Math. Mech 3 (2011) 1
- [47] A.O. Krushynska, V.G. Kouznetsova, M.G.D. Geers, *Visco-elastic effects on wave dispersion in three-phase acoustic metamaterials* J. Mech. and Phys. of Solids 96 (2016) 29
- [48] G. Carbone, C. Putignano, *A novel methodology to predict sliding and rolling friction of viscoelastic materials: Theory and experiments*, J. Mech. and Phys. of Solids 61 (2013) 1822
- [49] E. Absi, W. Prager, *Comparison of equivalence and finite element methods*, Comp. Methods. in Appl. Mech. Eng. 6 (1975) 59
- [50] S.M. Rubinstein, G. Cohen, J. Fineberg, *Dynamics of Precursors to Frictional Sliding*, Phys. Rev. Lett. 98 (2007) 226103
- [51] O. Ben-David, G. Cohen, J. Fineberg, *The Dynamics of the Onset of Frictional Slip* Science 330 (2010) 211
- [52] I. Svetlizky, J. Fineberg, *Classical shear cracks drive the onset of dry frictional motion*, Nature 509 (2014) 205

- [53] I. Svetlizky, D. Pino Munoz, M. Radiguet, D. S. Kammer, J. F. Molinari, J. Fineberg, *Properties of the shear stress peak radiated ahead of rapidly accelerating rupture fronts that mediate frictional slip*, PNAS 113 (2016) 542-547
- [54] E. Bayart, I. Svetlizky, J. Fineberg, *Fracture mechanics determine the lengths of interface ruptures that mediate frictional motion* Nature Physics 12 (2016) 166
- [55] D.S. Kammer, M. Radiguet, J.P. Ampuero, J.F. Molinari, *Linear elastic fracture mechanics predicts the propagation distance of frictional slip*, Tribol. Lett. 57 (2015) 23
- [56] M. Radiguet, D.S. Kammer, P. Gillet, J.F. Molinari, *Survival of heterogeneous stress distributions created by precursory slip at frictional interfaces*, Phys. Rev. Lett. 111 (2013) 164302
- [57] N. Lapusta, J.R. Rice, *Nucleation and early seismic propagation of small and large events in a crustal earthquake model* J. Geophys. Res. 108 (2003) 2205
- [58] M. Urbakh, J. Klafter, D. Gourdon, J. Israelachvili *The nonlinear nature of friction*, Nature 430 (2004)
- [59] B. He, W. Chen, Q.J. Wang, *Surface Texture Effect on Friction of a Microtextured Poly(dimethylsiloxane) (PDMS)*, Trib. Lett. 31 (2008) 187
- [60] N.B. Tay, M. Minn, S.K. Sinha, *A Tribological Study of SU-8 Micro-Dot Patterns Printed on Si Surface in a Flat-on-Flat Reciprocating Sliding Test* Trib. Lett. 44 (2011) 167
- [61] C. Greiner, M. Schafer, U. Pop, P. Gumbsch, *Contact splitting and the effect of dimple depth on static friction of textured surfaces*, Appl. Mater. Interfaces 6 (2014) 7986